JGR Oceans

RESEARCH ARTICLE
10.1029/2024JC021140

Influence of the Southern Hemisphere Supergyre on Antarctic Intermediate Water Properties in CMIP6 Models

Ophélie Meuriot[1], **Camille Lique**[2], **and Yves Plancherel**[1]

[1]Earth Science and Engineering, Imperial College London, London, UK, [2]Laboratoire d'Océanographie Physique et Spatiale (LOPS), Univ. Brest, CNRS, IRD, Ifremer, IUEM, Brest, France

Key Points:

- The supergyre is present at the depth of Antarctic Intermediate Water (AAIW) in CMIP6 models although the connectivity between basins differs across models
- AAIW core properties found within the supergyre tend to be homogenized across the different basins
- Climate change results in an intensification poleward shift and area reduction of the supergyre at intermediate depths

Supporting Information:

Supporting Information may be found in the online version of this article.

Correspondence to:

O. Meuriot,
ophelie.meuriot14@imperial.ac.uk

Citation:

Meuriot, O., Lique, C., & Plancherel, Y. (2024). Influence of the Southern Hemisphere supergyre on Antarctic intermediate water properties in CMIP6 models. *Journal of Geophysical Research: Oceans*, *129*, e2024JC021140. https://doi.org/10.1029/2024JC021140

Received 22 MAR 2024
Accepted 12 NOV 2024

Author Contributions:

Conceptualization: Ophélie Meuriot, Camille Lique, Yves Plancherel
Formal analysis: Ophélie Meuriot
Investigation: Ophélie Meuriot
Methodology: Ophélie Meuriot, Camille Lique, Yves Plancherel
Supervision: Camille Lique, Yves Plancherel
Writing – original draft: Ophélie Meuriot
Writing – review & editing: Ophélie Meuriot, Camille Lique, Yves Plancherel

Abstract The supergyre in the Southern Hemisphere is thought to connect the Atlantic, Indian, and Pacific subtropical gyres together. The aim of the study is to investigate whether the supergyre is identifiable in the Coupled Model Intercomparison Project Phase 6 (CMIP6) models and in the Estimating the Circulation and Climate of the Ocean (ECCO) reanalysis and to evaluate the influence of the supergyre on the properties of Antarctic Intermediate Water (AAIW), the dominant water mass at intermediate depths in the Southern Hemisphere. CMIP6 models and ECCO are in agreement at the surface with supergyres connected across all basins but present some differences at depth in both position and strength. AAIW core properties (temperature and salinity) present a high degree of similarity across basins within the supergyre but not outside of it. By the end of the century, the supergyre reduces in size and intensifies at intermediate depths, and the AAIW core depth warms in all basins and freshens in the Pacific although no clear trend in salinity can be found in the Atlantic and Indian basins in the SSP5-8.5 scenario. The high degree of similarity across basins within the supergyre is maintained in the future scenario. The results suggest that by connecting the basins together at intermediate depth, the supergyre plays a key role in circulating and homogenizing the AAIW core properties. Our results emphasize the role of the supergyre in circulating water masses at the surface and intermediate depths in CMIP6 models and hence its importance to the global circulation.

Plain Language Summary The Southern Hemisphere subtropical gyres (circular ocean currents driven by wind) in the Atlantic, Indian, and Pacific basins are thought to be connected together via a supergyre. The aim of the study is to assess whether the supergyre is identifiable in the latest state of the art climate models, the Coupled Model Intercomparison Project Phase 6 (CMIP6) models. In addition, the aim is to assess whether the inter basin connection due to the presence of the supergyre has an influence on the properties of Antarctic Intermediate Water (AAIW), the dominant water mass at intermediate depths in the Southern Hemisphere. The results show that the supergyre can be identified in CMIP6 models both at the surface and intermediate depths, although the connectivity between the Pacific and Indian basins varies across models. The AAIW core properties are found to present more similarity within the supergyre, and hence the results suggest that there is an increased homogenization of AAIW due to the water mass being circulated between the three basins. In the future, the supergyre is found to intensify and shift poleward as well as to reduce in size. However, the homogenization of the AAIW properties across the three basins is maintained.

1. Introduction

In the Southern Hemisphere, the wind-driven subtropical gyres in the Atlantic, Indian, and Pacific basins are connected together via a supergyre (Qu et al., 2019; Ridgway & Dunn, 2007; Roemmich et al., 2007; Speich et al., 2007). The position, extent, and intensity of the supergyre are thought to vary with depth. Ridgway and Dunn (2007) found that in the CSIRO Atlas of Regional Seas (CARS), the supergyre is located closer to the equator and connected via the Indonesian Throughflow (ITF) at the surface whereas at intermediate depths, the supergyre tends to be located further south and connected via the Tasman leakage (TL). It remains unclear down to what depth the supergyre is connected across all basins. The importance of the TL to the overturning circulation has been suggested in the literature (Rosell-Fieschi et al., 2013; Rousselet et al., 2020; Speich et al., 2002). Based on a Lagrangian analysis using Estimating the Circulation and Climate of the Ocean (ECCO), Rousselet et al. (2020) found that 49% of the northward flow across 6°S in the Atlantic (13.6 Sv) comes from the TL compared to 15% from Drake Passage and 35% from ITF. Speich et al. (2002) showed that in 3 general circulation models, the Tasman outflow is a key feature of the transport of Subantarctic Mode Water (SAMW) and Antarctic Intermediate Water (AAIW) south of Australia, which both contribute to the upper branch of the meridional

overturning circulation. The importance of the TL in the transport of intermediate waters was also revealed from the analysis of the velocity flow at 1,000 m depth inferred from Argo floats displacement (Rosell-Fieschi et al., 2013). Rosell-Fieschi et al. (2013) estimated a mean transport of intermediate waters through the TL of 3.8 ± 1.3 Sv from the Pacific to the Indian basins between March 2006 and December 2013.

Antarctic Intermediate Water (AAIW) is the dominant water mass at intermediate depths in the Southern Hemisphere and is characterized by a mid-depth salinity minimum. AAIW forms in the Southern Ocean and spreads northward in the Atlantic, Pacific, and Indian basins. AAIW likely plays a key role in the global water cycle by contributing to the return flow of freshwater from high latitudes dominated by precipitation to low latitudes dominated by evaporation (Carmack, 2007). AAIW is transported by the supergyre, which is thought to be primarily found at surface and intermediate depths (Ridgway & Dunn, 2007). Duan et al. (2013) investigated the water mass variability within the mid-depth supergyre in the Simple Ocean Data Assimilation (SODA) ocean reanalysis, focusing on the depth corresponding to the isopycnal surfaces of AAIW and SAMW (between 400 and 1,500 m) and found a supergyre structure encompassing the Atlantic, Pacific, and Indian basins. Given the presence of the supergyre circulation at intermediate depths, one may question what the influence of the supergyre is on AAIW properties and circulation. Ridgway and Dunn (2007) investigated the role of the Pacific/Indian coupled gyre on the distribution of SAMW and AAIW using the CARS atlas. In agreement with the results from the modeling study by Speich et al. (2002), Ridgway and Dunn (2007) found that AAIW circulates around the Pacific/Indian coupled gyre. The distribution of AAIW in the Atlantic is however not investigated in their study as the focus was set on the Pacific/Indian coupled gyre, which is found to have a stronger connection than the Atlantic/Pacific coupled gyre (Ridgway & Dunn, 2007).

Previous studies have assessed the historical variability and trends of the supergyre over the last decades based on observations and ocean reanalyses (Duan et al., 2013; Qu et al., 2019). Based on an analysis of the SODA ocean reanalysis, Duan et al. (2013) found that between 1958 and 2007, the supergyre at mid-depth (400–1,500 m) shifted poleward in response to an intensification and poleward shift of the westerly winds. The largest shift is found in the South Pacific where the edge of the supergyre shifts by 2.5° poleward. Similarly, Qu et al. (2019) found a strengthening of the supergyre with an increase of the transports associated with the Agulhas leakage (AL) and TL in the upper 2,000 m of around 2 Sv per decade between 1992 and 2016 in ECCO associated with a poleward shift of the westerly winds. A poleward shift and intensification of the supergyre can lead to increased exchanges between basins, which could have further implications on properties of the water masses advected within the gyre. Indeed, Biastoch et al. (2009) showed that an increase in AL in a high-resolution ocean model contributed to the increase in salinity in thermocline waters in the South Atlantic between 1968 and 2004. It remains unclear if the supergyre intensification and poleward shift are also identifiable at intermediate depths, and what the implications on AAIW could be. In addition, there is a need to investigate whether the trends identified in the historical period will persist in the future.

Coupled Model Intercomparison Project Phase 6 (CMIP6) climate models enable to investigate the long-term response of oceans to different climate scenarios (Eyring et al., 2016). However, a limited number of studies have investigated how the supergyre is represented globally in CMIP models. G. Wang and Cai (2013) found an increase in the wind stress curl at midlatitudes in the Southern Hemisphere in CMIP3 and CMIP5 models and suggested that it led to an increase and poleward shift of the supergyre. In addition, large uncertainties remain on the representation of intermediate waters in CMIP models in the Southern Hemisphere. Sallée et al. (2013) found that the mode and intermediate layers present large biases in temperature and salinity based on zonally averaged properties at 30°S in 21 CMIP5 models. F. Wang et al. (2023) found that AAIW presents a warm and salty bias in the Atlantic, which increases with the CMIP project phase (based on a multi-model average of 11 CMIP3, 11 CMIP5, and 11 CMIP6 models). Meuriot et al. (2022) showed that the biases are not uniform across basins in UKESM1-0-LL, the Met Office Hadley Center contribution to CMIP6. The AAIW core in UKESM1-0-LL presents a large spatial variation in salinity compared to observations with a salty bias in the Atlantic Basin (0.3 psu), a fresh bias in the west and east Pacific (−0.2 and −0.4 psu respectively), and no salinity bias in the Indian Basin.

The aim of the present study is to investigate how the circulation and properties of AAIW may be influenced by the supergyre in CMIP6 models. The hypothesis is that the presence of a supergyre connecting the Atlantic, Indian, and Pacific basins could homogenize properties at intermediate depths. However, it is unclear if the supergyre is present in CMIP6 models and what its vertical structure is and hence there is a need to assess and

quantify the main characteristics of the supergyre in CMIP6 models. The paper is structured as follows. Section 2 describes the data sets as well as the methods used in this study to quantify both the supergyre and AAIW properties. Section 3 focuses on the vertical structure of the supergyre, looking at the differences in position and strength of the supergyre with depth in CMIP6 models and in the ECCO reanalysis. Section 4 investigates the linkages between AAIW properties and the supergyre at mid-depth in both ECCO and CMIP6 models. Section 5 focuses on the future changes in mid-depth supergyre and AAIW properties. Conclusions are given in Section 6.

2. Data Sets and Methods

2.1. CMIP6 Models

We use data from the CMIP6 historical and ScenarioMIP simulations. For the historical period, we have selected 39 models based on the availability of the potential temperature (*thetao*), salinity (*so*), eastward (*uo*), and northward velocities (*vo*) ocean monthly variables. Information on the different model components (ocean, atmosphere, and sea-ice models) as well as references for each model are given in Table S1 in Supporting Information S1. Further information about the CMIP6 protocol can be found by Eyring et al. (2016). The variables are averaged between 1992 and 2011 to compare to the ECCO data set (see Section 2.2) and interpolated on a regular 360 × 180 (latitude × longitude) grid using the Climate Data Operators (CDO) tools (Schulzweida, 2022). We build a climatology based on a 20 years time period (1992–2011) in order to average over several phases of the main natural modes of variability in the Southern Hemisphere such as the El Niño Southern Oscillation (ENSO) or Southern Annular Mode (SAM).

Simulations run under Shared Socioeconomic Pathway 5-8.5 (SSP5-8.5), which corresponds to the highest radiative forcing scenario, are used to compare to the historical simulations. SSP5 corresponds to the category of scenario with fossil fuel development and the 8.5 corresponds to the 2,100 forcing level (W\m^2) with the mean surface temperature increase expected to reach 5°C by 2,100 (O'neill et al., 2016). The 22 models for which the required ocean monthly variables are available in the SSP5-8.5 scenario are shown in Table S1 in Supporting Information S1.

2.2. ECCO Reanalysis

The ECCO reanalysis Version 5 data set combines an ocean circulation model with remotely sensed data and in situ data constraints (Forget et al., 2015; Zhang et al., 2018). Model outputs are available from 1992 to 2017 and run on a LLC270 grid with a horizontal spacing varying between 12 km at high latitudes to 37 km at the equator and 50 vertical levels. Monthly outputs over the period 1992–2011 are averaged month by month to obtain a climatological year. The model fields are further interpolated on a regular 360 × 180 (latitude × longitude) to match with the processing of the CMIP6 model data. Further information on the ECCO data set can be found by Zhang et al. (2018). The AAIW core depth and salinity in ECCO was compared to the WOA18 climatology and found to provide a suitable representation of the mean AAIW core properties (Figure S1 in Supporting Information S1). Estimating the Circulation and Climate of the Ocean is used here as a reference against which to compare the CMIP6 models ECCO also has matching velocity fields, which are needed to investigate the circulation in the Southern Hemisphere.

2.3. Definition of the Antarctic Intermediate Water Core Properties

The depth of the core of AAIW is calculated following the method described by Meuriot et al. (2022) using the mean salinity field. At each grid point, the depth of the vertical salinity minimum (represented in black dots in Figure 1, panel a for ECCO) between the maximum monthly mixed layer depth (maximum value found during a climatological year) and 2,000 m (upper and lower red dashed lines respectively in Figure 1a) is identified. Locations where the salinity minimum is found at the depth of the maximum mixed layer depth or at 2,000 m are masked out (white areas in Figure 1b). The white area in the southeast Pacific corresponds to a region where the AAIW core is not detected by our method and where the shallower South East Pacific Intermediate Water is present (Emery et al., 2001; Meuriot et al., 2022). The depth of 2,000 m is chosen based on observations as the salinity minimum is shallower than this depth in all basins. The maximum mixed layer depth is calculated from the monthly climatological field of density using a density threshold criterion of 0.125 kg/m^3, following the criteria of de Boyer Montégut et al. (2004) and Jiao et al. (2022). The salinity, temperature, and density at the depth of the salinity minimum define the properties of the AAIW core. Using properties representative of the

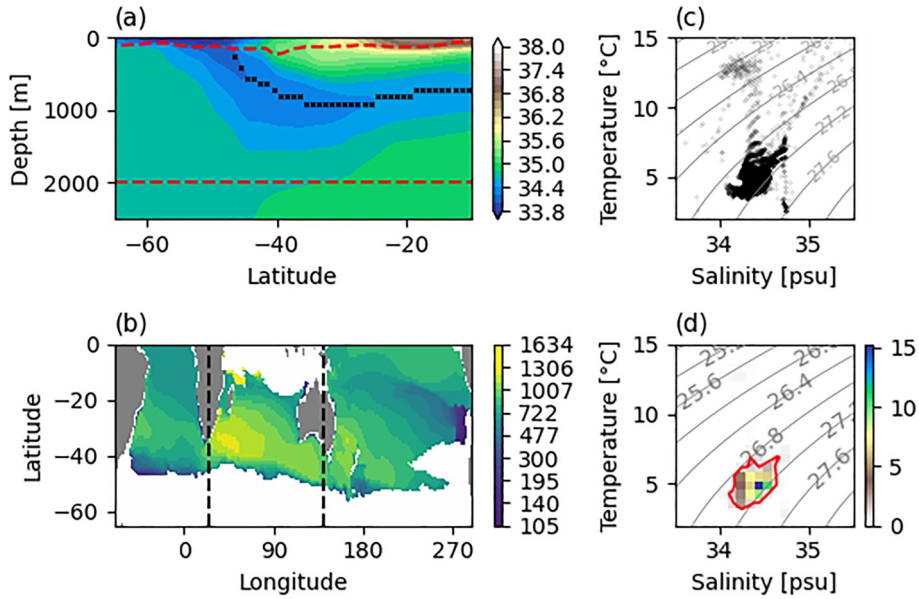

Figure 1. Illustration of the metrics and definitions used to describe Antarctic Intermediate Water (AAIW) applied to the Estimating the Circulation and Climate of the Ocean reanalysis. (a) Salinity section (psu) in the Atlantic Ocean (20°W). The black dots show the AAIW core defined as the vertical salinity minimum between the maximum mixed layer depth and 2,000 m (upper and lower red dashed lines, respectively). (b) Map of the AAIW core depth (m) with white areas corresponding to regions where the AAIW core is not detected. The vertical black lines indicate where the Atlantic, Indian, and Pacific basins are divided. (c) Temperature/Salinity (T/S) diagram at the core of AAIW in the Southern Hemisphere. (d) Point density of the T/S values shown in panel (c) per 0.65°C × 0.1 psu bin where the red line corresponds to the 1% contour (see Section 2.3 for further detail on the methodology).

AAIW core itself rather than at a fixed depth or on fixed isopycnals helps to compare the properties of the AAIW core across models irrespective of model biases and differences.

We further aim to define an outline of the T/S core properties of AAIW. Temperatures and salinity of the AAIW core in the Southern Hemisphere are shown in a T/S (Temperature/Salinity) diagram for ECCO in Figure 1c. The density of T/S points is calculated per bin of 0.65°C × 0.1 psu (color in Figure 1d). A point density value of 1% is here used to delimit the region corresponding to AAIW's core T/S values (red contour in Figure 1d). Using an outline to define the T/S values of AAIW core is helpful for visualization purposes as multiple outlines can be overlaid and hence AAIW's properties can be compared across different regions. The methodology will be used in Sections 4 and 5 to compare AAIW's core properties in the Atlantic, Pacific, and Indian basins.

2.4. Definitions of the Supergyre Metrics

To compare the properties of the supergyre between models as well as between depths, we define metrics such as the supergyre strength, area, and southern boundary. These supergyre metrics are derived from a depth-integrated streamfunction defined as:

$$\psi_{xy}(x,\, y) = -\int_{y'}^{y}\int_{l1}^{l2} u\left(x, y', z\right)\, dz\, dy'$$

where u is the eastward velocity, $l1$ and $l2$ are the depth boundaries selected for the analysis. y' is set on the Antarctic continent where the velocity is 0.

The aim is to assess how the supergyre varies with depth. Ridgway and Dunn (2007) based their analysis on the mean steric height computed for different layers (0–2,000 m, 0–400 and 1,000 m–2,000 m). In Qu et al. (2019), the streamfunction was calculated from top to bottom as well as in the upper 500 m and between 500 and 1,500 m. Similarly to Ridgway and Dunn (2007) and Qu et al. (2019), we define surface, intermediate, and deep layers to assess how the supergyre varies vertically. As different models present different biases, the layers are defined

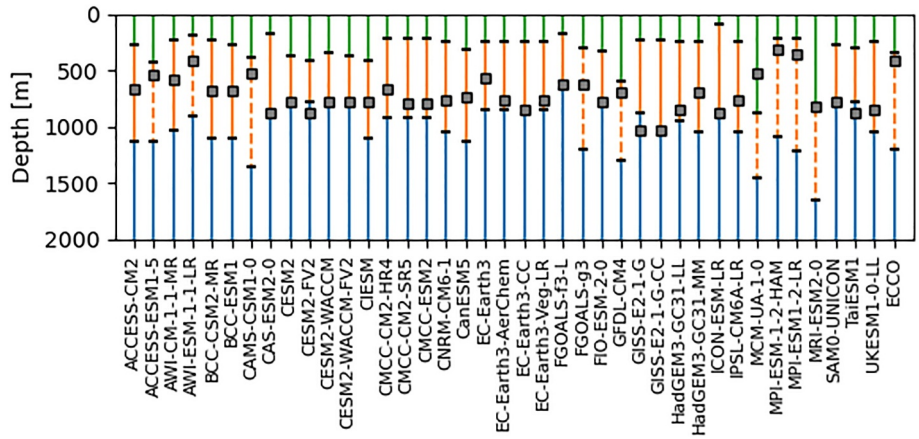

Figure 2. Depth range covered by the surface (green), intermediate (orange), and deep (blue) layers in CMIP6 models and Estimating the Circulation and Climate of the Ocean. The dashed lines show models for which the supergyre is on average disconnected between the Indian and Pacific basins in the intermediate layer. The gray squares show the depth at which the supergyre disconnects between the Indian and Pacific basins.

individually for each model. The intermediate layer is centered around the AAIW core with the upper and lower boundaries defined as the 0.05 (0.95) percentile value of the AAIW core depth (calculated from the time averaged salinity) between 60°S and 20°S. These latitudes are selected to encompass the domain where the supergyre can be found. The surface layer is defined as the layer between the ocean surface and the upper intermediate layer boundary, and the deep layer is defined as the layer between the lower intermediate layer boundary and 2,000 m. 2,000 m is selected as the deep boundary in all models similarly to Ridgway and Dunn (2007). Figure 2 shows the depth range of the surface, intermediate, and deep layers for each model in green, orange, and blue, respectively.

The contour of the supergyre for a given layer corresponds to the best-fit streamfunction contour calculated in two steps, as illustrated in Figure 3. (a) For each longitude, we find the minimum value in streamfunction, which is crossed at two latitudes exactly (black dashed line in Figure 3b) and hence corresponds to a closed gyre at that longitude. (b) The largest of the values from (a) (black contour in Figure 3a) is selected as the outline of the supergyre.

The contour corresponding to the outline of the supergyre is defined for the surface, intermediate, and deep layers. The supergyre strength is the value of the contour of the supergyre outline normalized by the layer thickness and has units of Sv/m. The normalization is required to take into account the varying thicknesses of the layers between models (Figure 2) and to hence compare the values across the different models. The area of the supergyre is calculated as the area within the supergyre contour, and the southern boundary is defined as a zonal average of the southernmost boundary of the supergyre.

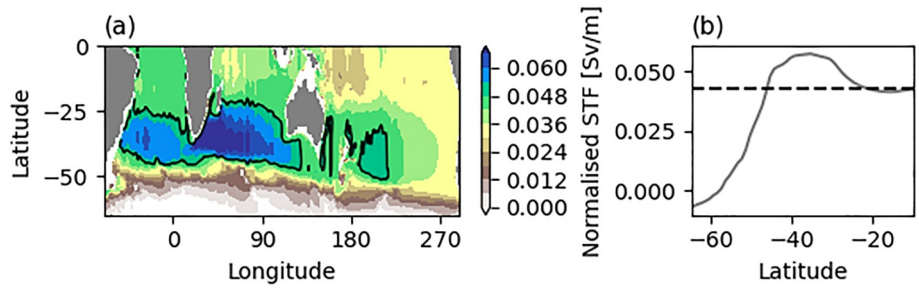

Figure 3. Illustration in Estimating the Circulation and Climate of the Ocean (ECCO) of the supergyre definitions and metrics applied to the ECCO reanalysis. (a) Layer-integrated streamfunction for the intermediate layer normalized by the layer thickness (Sv/m). The black contour shows the normalized streamfunction contour selected to delimit the supergyre. (b) Zonal variations of the normalized streamfunction along a section in the Atlantic Ocean (20°W). Further details on the methodology can be found in Section 2.4.

3. Variations of the Supergyre Properties With Depth

The aim of this section is to assess how the structure of the supergyre varies with depth in CMIP6 models. The supergyre properties (position, strength, area, and southern boundary) are calculated for the surface, intermediate, and deep layers as defined in Section 2.4 in all the individual CMIP6 models (for the historical simulations) and in ECCO.

3.1. Supergyre Position and Connectivity

In ECCO and in all CMIP6 models, the supergyre at the surface is connected via the AL between the Atlantic and Indian basins and via the ITF and TL between the Indian and Pacific basins (Figure 4, green contour). The supergyre contour follows closely the zero wind stress curl contour (Figure 4, black dashed contour). G. Wang et al. (2014) highlight that the zero wind stress curl is an indicator of the boundary between the supergyre and the Antarctic Circumpolar Current (ACC).

At intermediate depths, the southern supergyre boundary (orange contour in Figures 4, 5c, and 5f) matches closely the southern boundary at the surface in both ECCO and CMIP6 models. The supergyre in the intermediate layer exhibits a reduced northward extent in the Atlantic, Indian, and Pacific basins as well as a reduced eastward extent in the Pacific compared to the supergyre at the surface in both ECCO and CMIP6 models. In contrast with the surface, the supergyre contour for the intermediate layer does not go through the ITF in any of the models. Although the supergyre can be identified for the intermediate layer in all CMIP6 models and in ECCO, differences between them are visible in terms of connectivity between the Indian and Pacific basins. In 30 out of 39 CMIP6 models, the supergyre is connected between all basins. In ECCO and in 9 CMIP6 models, the supergyre contour for the intermediate layer is broken between the Indian and Pacific basins, suggesting a disconnection between the Atlantic/Indian and Pacific basins. Lack of velocity field data at intermediate depths make it difficult to determine the level of supergyre connectivity from observations alone.

In the deep layer, the supergyre only covers small regions of the southeast Atlantic and southwest Indian basins (Figure 4, blue contour). The southern supergyre boundary is located further north in the deep layer compared to the surface and intermediate layers in both CMIP6 models and ECCO. The supergyre contour of the deep layer does not appear connected between any basins in ECCO and in 12 out of 39 CMIP6 models but remains connected between the Indian and Atlantic basins in the remaining CMIP6 models.

Our results suggest that in ECCO and CMIP6 models, wind drives the circulation for the surface and intermediate layers but exerts a limited influence on the deep layer. The supergyre can be identified in the intermediate layer, which corresponds to AAIW, although some differences in connectivity between Pacific and Indian basins are visible. The results are similar to the findings of Ridgway and Dunn (2007)), who found that the supergyre shifts poleward with depth with the supergyre connected through the ITF at the surface and through TL at depth. The disconnection between the Pacific and Indian basin was however not identified in their study. In the next subsections, the depth variation of the supergyre properties (area, strength, and southern boundary) as well as the connectivity between basins are assessed (Sections 3.2 and 3.3, respectively).

3.2. Correlation of Supergyre Properties Across Layers

The surface and deep supergyre properties are plotted against the intermediate supergyre properties (area, normalized strength, and zonal mean southern boundary) in Figure 5 to investigate whether a correlation exists across the models between the supergyre properties in the intermediate layer and the supergyre properties in the surface and deep layers. Note that the r and p values in this section correspond to the Pearson correlation coefficient and the p-value, respectively.

As noted in Section 3.1, the area is the largest at the surface and decreases with depth. Models with a smaller supergyre area for the intermediate layer tend to also have a smaller supergyre area for the surface and deep layers (Figure 5a) although the correlation is stronger between the supergyre's area in the surface and intermediate layers ($r = 0.87$) than between the deep and intermediate layers ($r = 0.47$). The range of values for the area is larger for the surface (73×10^6 km^2 to 123×10^6 km^2) and intermediate (28×10^6 km^2 to 80×10^6 km^2) layers than the deep layer (0.5×10^6 km^2 to 25×10^6 km^2). In ECCO (dashed line in Figure 5d), the supergyre area is smaller than in most models and is 90×10^6 km^2, 36×10^6 km^2 and 3×10^6 km^2 for the surface, intermediate, and deep layers, respectively.

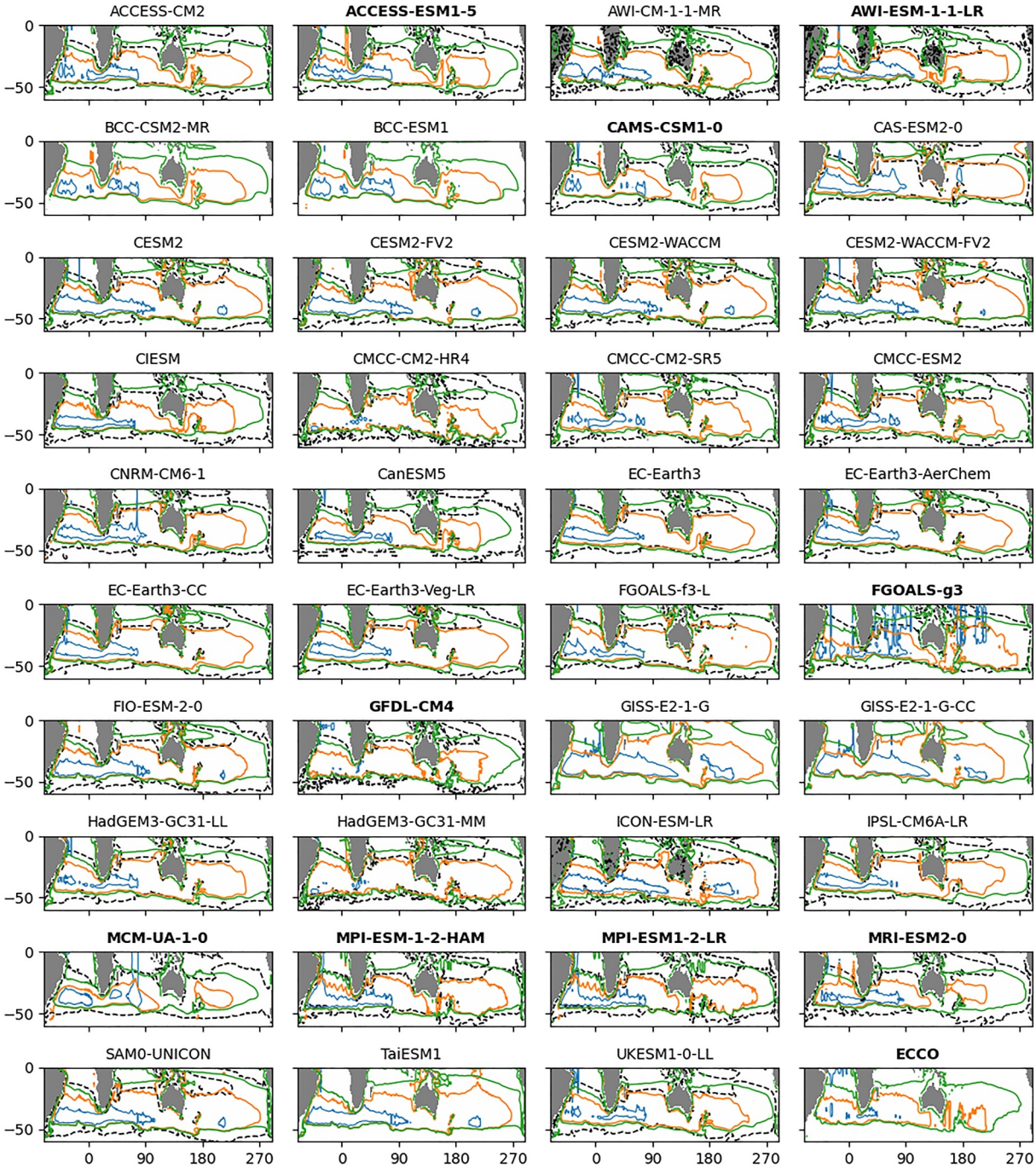

Figure 4. Supergyre contours for the surface (green), intermediate (red), and deep (blue) layers for CMIP6 models and Estimating the Circulation and Climate of the Ocean. The zero wind stress curl contour is shown as a black dashed line for the models for which the wind stress field was available. Bold titles correspond to models with a disconnected supergyre for the intermediate layer.

The supergyre normalized strength is strongest at the surface and reduces in the intermediate and deep layers. Similarly to the correlation with depth in supergyre area, the correlation between the surface and intermediate layers in normalized strength values is stronger ($r = 0.93$) than between the intermediate and deep layers ($r = 0.68$). The supergyre normalized strength in ECCO (dashed line in Figure 5e) fits well in the range of values found in models in the three layers with values of 0.05, 0.03, and 0.01 Sv/m in the surface, intermediate, and deep layers.

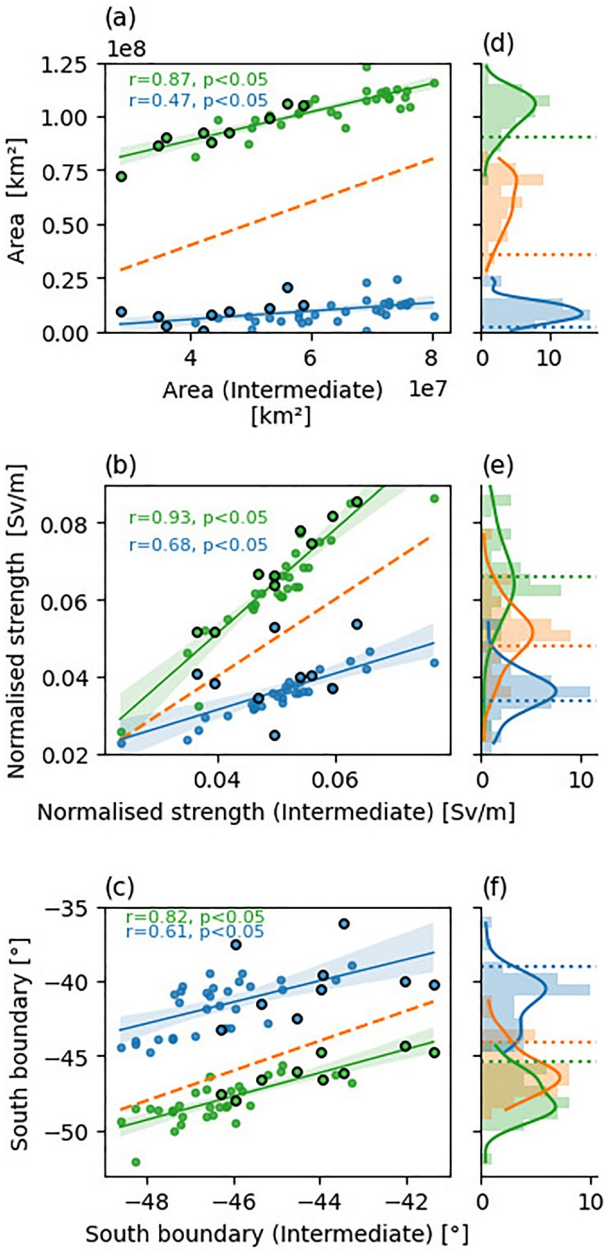

Figure 5. Supergyre surface and deep (a) area, (b) normalized strength, and (c) mean southern boundary plotted against the corresponding supergyre properties (orange dashed lines) in the intermediate layer in green and blue, respectively. The best fit line is calculated for CMIP6 models and the r (Pearson correlation coefficient) and p values are indicated. Black circles correspond to models for which the supergyre is disconnected in the intermediate layer. Panels (d–f) show histograms of CMIP6 areas, normalized strength, and mean southern boundary, respectively, for the surface (blue), intermediate (orange), and deep (green) layers. The horizontal dashed lines correspond to the supergyre properties in Estimating the Circulation and Climate of the Ocean.

The supergyre mean southern boundary for the surface layer is located between 44°S and 52°S in CMIP6 models. For the intermediate layer, the supergyre mean southern boundary is located further north with on average an equatorward shift of 1.7° compared to the supergyre position for the surface layer in CMIP6 models. For the deep layer, the supergyre is located on average 4.6° equatorward compared to the intermediate layer. The mean latitude of the southern boundary in the intermediate layer supergyre is correlated with the mean latitude of the southern boundary in the surface and deep layers (0.82 and 0.61, respectively). In ECCO, the supergyre mean southern boundary is located further north than in most models with means equal to 39°S, 44°S, and 46°S for the surface, intermediate, and deep layers, respectively.

3.3. Implications of Basin Connectivity on Supergyre Properties

The majority of CMIP6 models (30 out of 39 CMIP6 models) present a supergyre connected across all basins at intermediate depths whereas in ECCO and in 9 CMIP6 models, the supergyre appears disconnected between the Pacific and Indian basins at intermediate depths. The aim is to investigate if we can find a link between the differences in connectivity of the supergyre at intermediate depths and the supergyre properties.

As shown in Figure 5, models with a disconnected supergyre (circled in black) at intermediate depths tend to have smaller areas, and their southern boundary is located further north compared to models with a connected supergyre. However, the connectivity of the supergyre does not appear to be statistically related to the normalized strength values, as models with disconnected supergyres and connected supergyres are within the same range of values (Figure 5b). The correlation between the surface and intermediate layer supergyre strength appears to be enhanced for models with a disconnected supergyre (black circles in Figure 5b) with models with a disconnected supergyre located mostly above the best-fit line. Although the number of models is too small to obtain a statistically significant correlation, the results suggest that models with a disconnected supergyre at intermediate depths have a stronger supergyre at the surface than models with a connected supergyre.

The separation between the surface, intermediate, and deep layers provides a sufficient broadscale representation of the depth variability of the supergyre for the application presented here, but one should keep in mind that the three-layer system is a simplification of the supergyre structure. The supergyre can vary within a layer. We here explore how the supergyre connectivity varies by calculating a disconnection depth for each model as the last depth level at which the supergyre is connected between the Pacific and Indian basins. Results are shown as gray squares in Figure 2. In the majority of CMIP6 models (35 out of 39), the disconnection depth is within the intermediate layer. In CESM2-FV, GISS-E2-1-G-CC, and TaiESM1, the disconnection depth is located right below the intermediate layer and in MCM-UA-1-0, it is 360 m shallower than the upper boundary of the intermediate layer. The large gap between the intermediate layer and the disconnection depth found in MCM-UA-1-0 is likely due to the very low vertical resolution in this model (18 levels). Similarly to ECCO, models with a disconnected supergyre in the intermediate layer (shown with orange dashed lines in Figure 2) have a disconnection depth closer to the upper boundary of the intermediate layer. Although there are some differences across CMIP6 models and ECCO, the disconnection depth is found in the intermediate layer in the majority of models (apart from MCM-UA-1-0). Note that the connectivity between basins could occur through the

propagation of eddies, narrow boundary currents or intermittent features, which are not captured when using time averages and are likely not captured in CMIP6 and their typical low resolution.

We have shown that the supergyre can be identified at intermediate depths across CMIP6 models and ECCO, although some models present a disconnect between the Indian and Pacific basins. The degree of disconnection between the Indian and Pacific basins in the intermediate layer was found to vary within the layer and hence an exchange in properties could still be expected across all basins. Based on these results, the following section seeks to investigate whether the properties of the supergyre at intermediate depth has an influence on AAIW properties. We hypothesize that as the supergyre enables an exchange of properties across the three basins, a homogenization of the AAIW core properties could be identified.

4. Influence of the Supergyre on AAIW Properties

In this section, we focus on the supergyre position and properties at intermediate depths and their relationship with the AAIW core properties.

4.1. Linkages Between AAIW Spatial Patterns and Supergyre Position

The position of the supergyre in the intermediate layer (black contour in Figure 6) coincides closely to the spatial pattern of the AAIW core depth (color in Figure 6). The dashed black lines in Figure 6 show the streamfunction contours with increased values toward the center of the supergyre. In ECCO, the supergyre contour encompasses the region where the AAIW core is the deepest (800–1,400 m) with shallower core values found outside the supergyre. The depth of the AAIW core increases toward the center of the supergyre, with the deepest values coinciding with the largest streamfunction contour. The region where AAIW is deepest in ECCO and CMIP6 models coincides with the region where SAMW is thickest in observations (Feucher et al., 2019). The results are similar in CMIP6 models, with a close match between the position of the supergyre and AAIW core's depth contours and also with the largest streamfunction values corresponding to the deepest AAIW core within the supergyre. The pycnocline is expected to be deeper at the center of anticyclonic gyres in the Southern Hemisphere, hence the AAIW core is found at deeper depths.

The supergyre position (black contour in Figure 7) also coincides with spatial distribution of the salinity at the core of AAIW (color in Figure 7). In the Atlantic, the supergyre contour corresponds to a region where isohalines are close together, indicating a strong meridional salinity gradient. In the east Pacific, the supergyre contour delimits a region within the Pacific where the AAIW core is saltier than in the east part of the basin outside the supergyre. Although these patterns are consistent across most models, there are some exceptions. In CESM2, CESM2-FV2, CESM2-WACCM,CESM2-WACM-FV2, FGOALS-f3-L, SAM0-UNICON, and TaiESM1, the supergyre is larger than in most CMIP6 models, and the supergyre contour encompasses the low salinity region in the South East Pacific.

4.2. Variation of AAIW Core Properties in the Atlantic, Pacific, and Indian Basins

The temperature and salinity values at the depth of the AAIW core in the Southern Hemisphere are examined to assess the influence of the supergyre on the AAIW core properties in the Atlantic, Pacific, and Indian basins (in blue, orange, and green, respectively in Figure 8). The T/S values corresponding to the Atlantic, Pacific, and Indian basins present a high degree of overlap inside the supergyre (black dashed contour in Figure 8). In ECCO, the AAIW properties within the supergyre are found within the same density range (26.9–27.2 kg\m^3) with an overlap in T/S values between the Atlantic, Indian, and Pacific basins. Outside the supergyre, the AAIW core is less dense in the Pacific in ECCO. In addition, the AAIW core outside the supergyre in the Indian basin is saltier than within the supergyre. The overlap in T/S values between the different basins highlights a high level of homogeneity in AAIW core properties within the supergyre. The overlap of the AAIW core T/S values within the supergyre can also be identified within the CMIP6 models. For simplicity, only the outline of the T/S point values in each basin is shown but not the density of point. Hence, a small overlap area between basins could correspond to the T/S region with a high point density.

To investigate whether the homogenization in the AAIW core properties occurs within the supergyre or whether the AAIW core properties present a high degree of similarity between the different formation sites (or if there is a single formation site in some models), we compare the range of AAIW core properties at its origin and within the

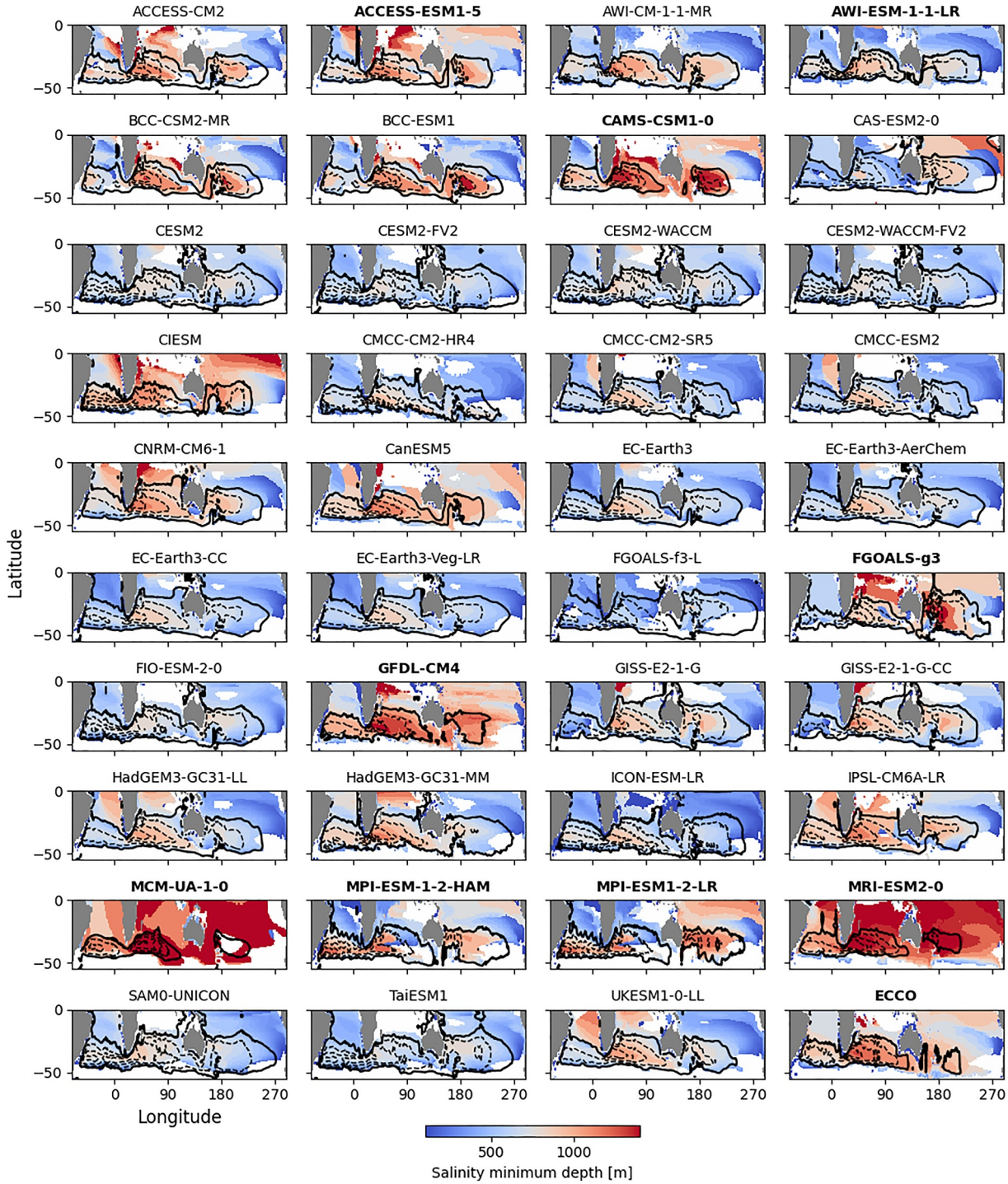

Figure 6. Antarctic Intermediate Water core depth (color) with the supergyre contour in the intermediate layer (black line) and streamfunction contours (black dashed lines) for CMIP6 models and Estimating the Circulation and Climate of the Ocean. Bold titles correspond to models with a disconnected supergyre.

supergyre. Figure 9 shows the variance in the AAIW T/S core properties at the location of the southernmost salinity minimum (position where the AAIW has newly formed) compared to the variance in the AAIW T/S core properties at the center of the intermediate supergyre (defined as the latitudinal position of the maximum streamfunction). A large difference in temperature variance can be found between the southernmost AAIW core and the mid-supergyre AAIW core with the mid-supergyre AAIW core presenting much smaller values. The salinity variance of the AAIW core is similar at the southernmost AAIW core compared to at the center of the

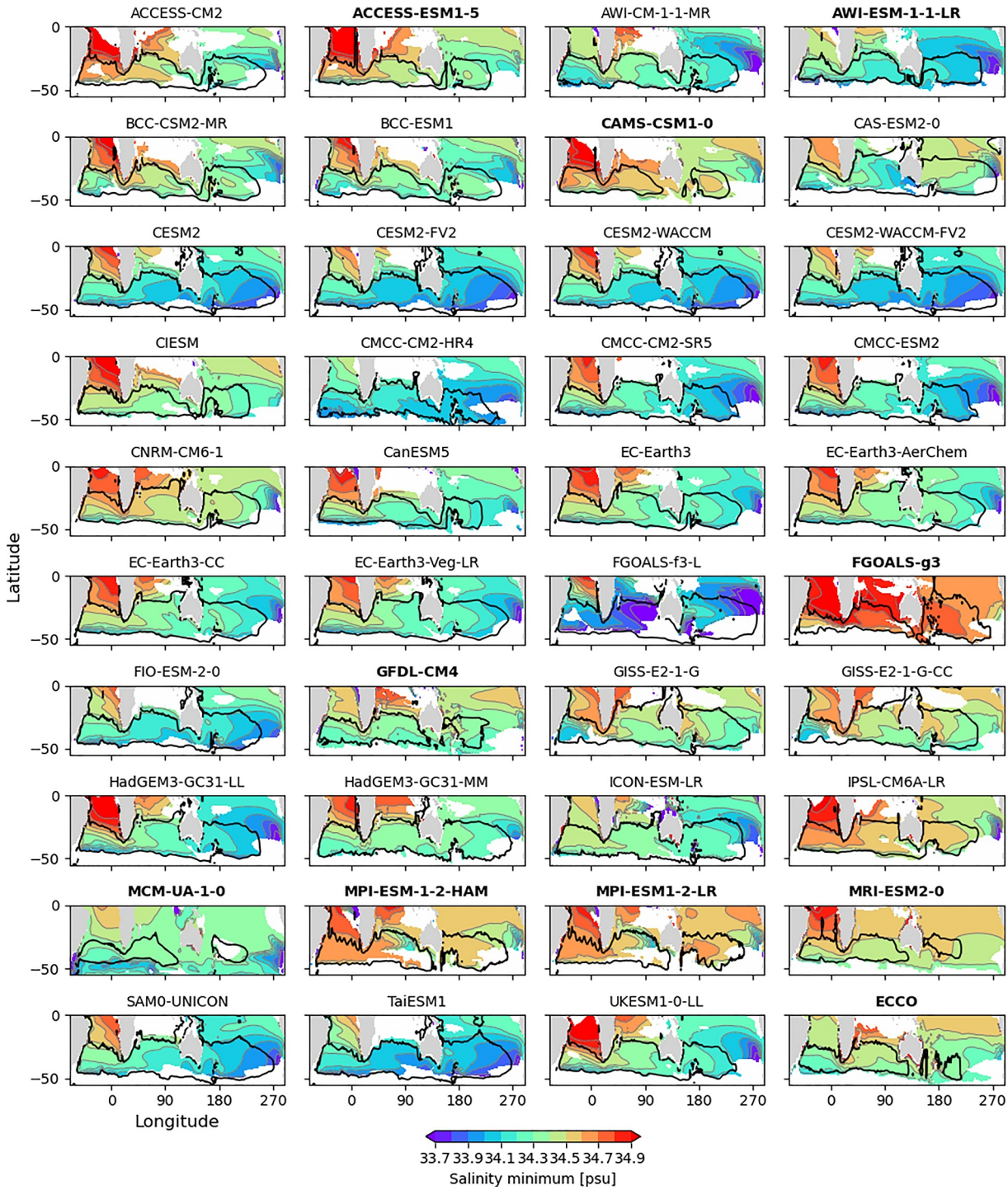

Figure 7. Antarctic Intermediate Water (AAIW) core salinity (color) and contours (gray lines every 0.1 psu) for CMIP6 models and Estimating the Circulation and Climate of the Ocean. The intermediate layer supergyre contour is represented by a black line. White areas represent regions where the AAIW core is not detected. Bold titles correspond to models with a disconnected supergyre.

supergyre, with 23 out of 39 CMIP models presenting a larger salinity variance at the southernmost AAIW core compared to at the center of the supergyre. The results overall show a striking difference in the variance in temperature between the southernmost AAIW core and the center of the supergyre with over half of the models presenting a smaller variance in salinity at the center of the supergyre. The results suggest that the supergyre does contribute to the homogenization of the AAIW core T/S properties.

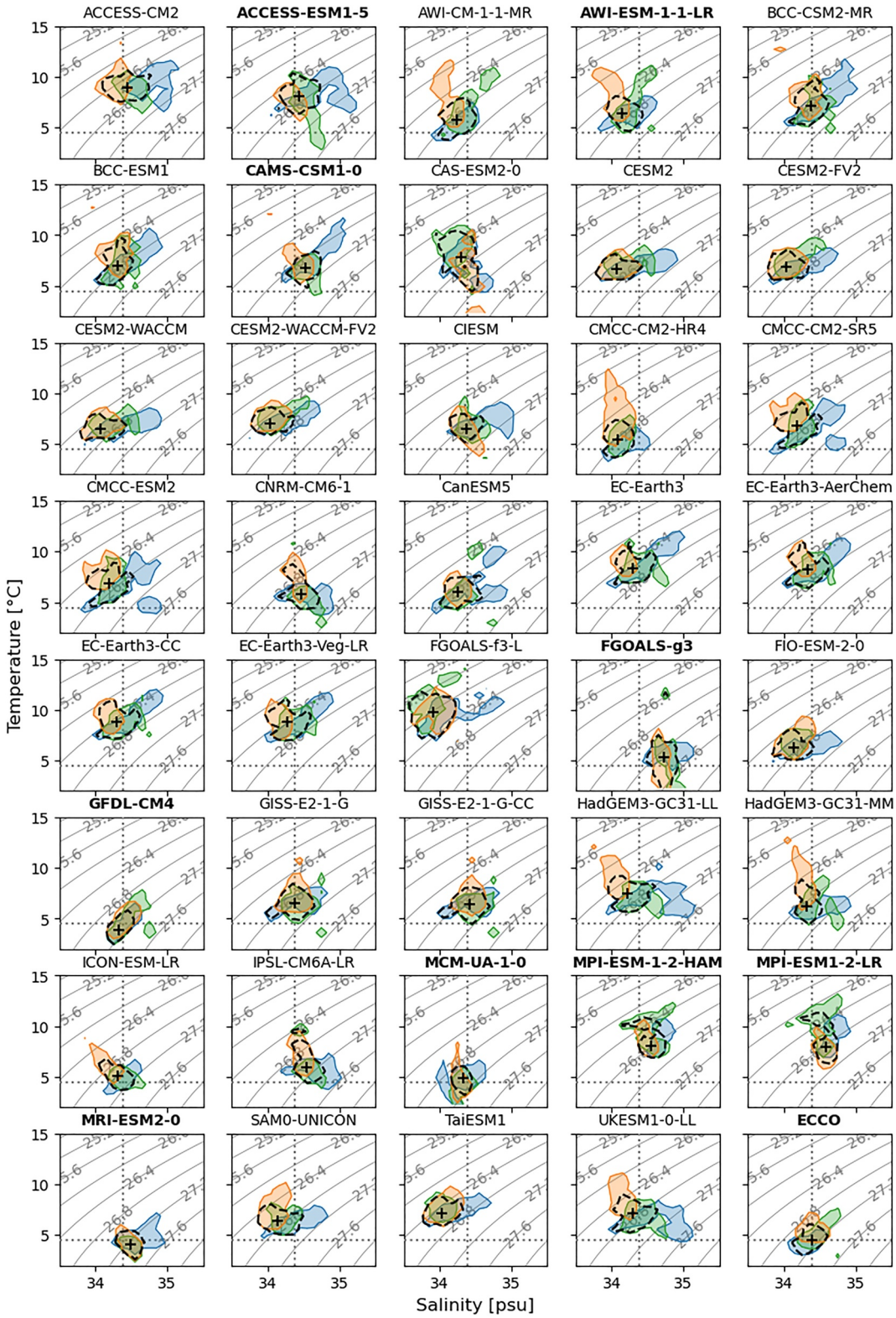

Figure 8. T/S diagram of the Antarctic Intermediate Water (AAIW) core temperature and salinity in the Pacific, Indian, and Atlantic basins (in orange, green, and blue, respectively) for CMIP6 models and Estimating the Circulation and Climate of the Ocean (ECCO). The black dashed line outlines the T/S values of the AAIW core within the supergyre. The median T/S value of the CMIP6 models is shown as a black cross with the horizontal and vertical gray dotted lines representing the median temperature and salinity values, respectively, in ECCO. Bold titles correspond to models with a disconnected supergyre.

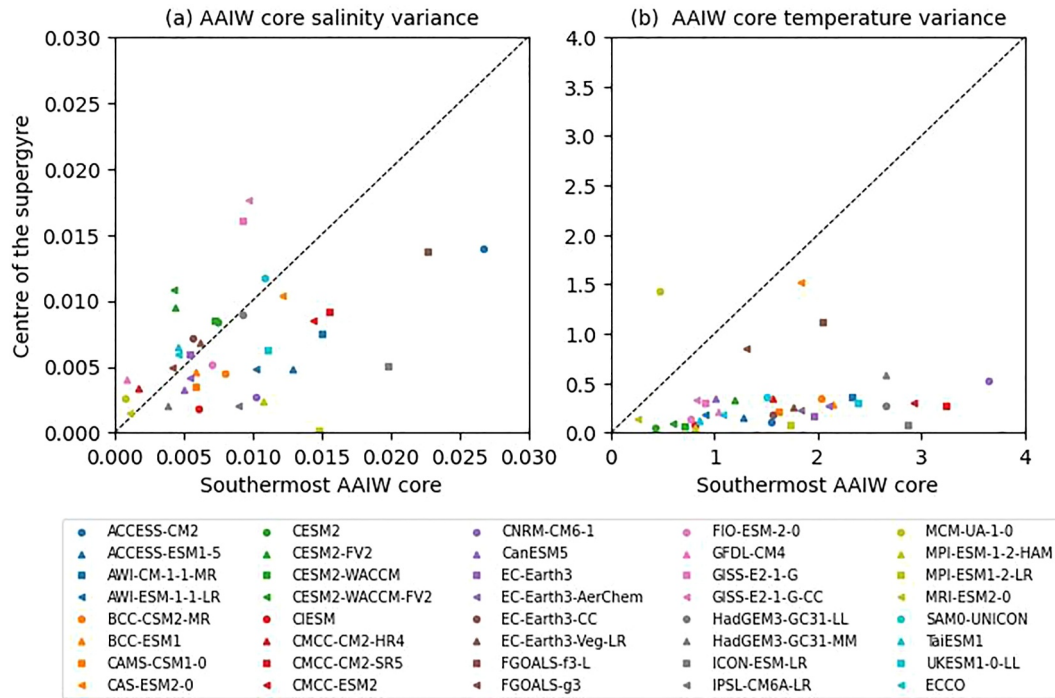

Figure 9. (a) Salinity and (b) temperature variance at the southernmost Antarctic Intermediate Water core (*x* axis) compared to at the center of the supergyre (defined as the latitudinal position of the maximum streamfunction.

Although CMIP6 models are able to represent the overlap of the AAIW core T/S values within the supergyre in the Atlantic, Indian, and Pacific basins, all the CMIP6 models present a bias compared to ECCO evident when examining the median T/S values of the AAIW core inside the supergyre (Figure 8). The AAIW core within the supergyre in 37 out of 39 models exhibits a warm bias compared to ECCO. 26 out of 39 CMIP6 models present a salty bias compared to ECCO, whereas 9 out of 39 CMIP6 models present a fresh bias and 4 CMIP6 models (BCC-CSM2-MR, CIESM, GIESM-E2-1-G, and GIESM-E2-1-G-CC) present similar median salinity values compared to ECCO.

In contrast to the AAIW properties found within the supergyre for which the basin to basin differences in AAIW core properties are small, the AAIW properties outside the supergyre present larger heterogeneity between basins. In the remainder of the section, we compare the properties at the core of AAIW outside of the supergyre up to the equator. In ECCO, north of the supergyre, the AAIW core is at a similar temperature in the three basins (between 4°C and 7°C) but differs in salinity with a fresher AAIW core in the Pacific (between 34.1 and 34.3 psu) and a saltier core in the Indian Basin (between 34.5 and 34.7 psu). Although CMIP6 models present a similar pattern with a fresher AAIW core in the Pacific and saltier AAIW core in the Indian/Atlantic, the basin to basin difference in T/S values has a larger spread. As a consequence, there is also a striking difference in the range of density values found in each CMIP6 model. The large spread in AAIW core properties found outside the supergyre highlight the CMIP6 models' deficiency in maintaining the AAIW properties as it spreads northward of the supergyre. Although the northward propagation of AAIW north of the supergyre is outside of the scope of the study, the results highlight the need to assess the mechanisms associated with the large biases found at low latitudes (between 20°S and the equator) in CMIP6 models.

5. Future Changes in Supergyre and AAIW Properties

This section focuses on the changes in supergyre and AAIW properties between the historical period (1992–2011) and the SSP5-8.5 scenario averaged between 2081 and 2100 in 22 CMIP6 models (see Table S1 in Supporting Information S1). The aim is to assess how the supergyre properties in the intermediate layer and the AAIW core properties respond to climate change.

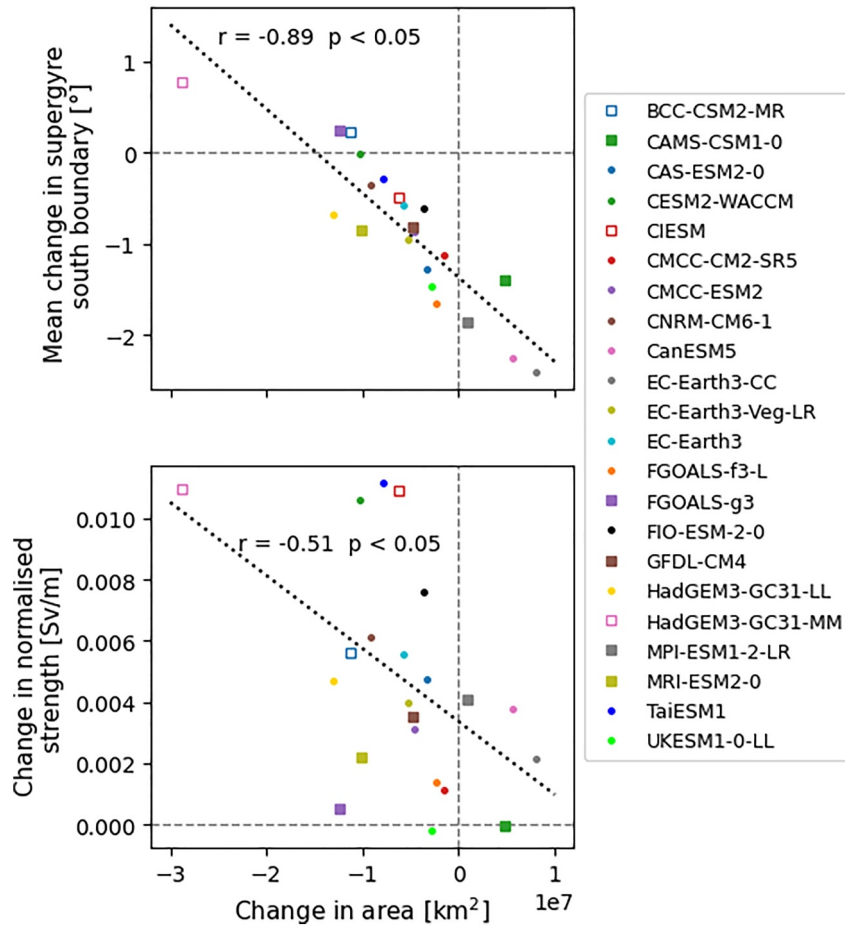

Figure 10. Changes in supergyre mean southern boundary (top) and in normalized strength (bottom) against changes in area for the intermediate layer between the SSP5-8.5 simulation and the historical simulation in the CMIP6 models. Square (circle) markers correspond to models with a disconnected (connected) supergyre in the SSP5-8.5 scenario with the unfilled squares corresponding to models for which the supergyre was connected across all basins in the historical simulation. The best fit line is shown in black dots.

5.1. Future Changes of the Supergyre Properties

In a warmer climate, the supergyre at intermediate depths reduces in area in most models with the exception of MPI-ESM1-2-LR, CanESM5, EC-Earth3-CC, and CAMS-CSM1-0 (Figure 10). The reduction in area is mainly visible in the Indian and Pacific basins but remains limited in the Atlantic Basin (Figure 11). The mean supergyre southern boundary shifts poleward in 18 out of the 22 CMIP6 models (Figure 10) but not in BCC-CSM2-MR, CESM2-WACCM, FGOALS-g3, and HadGEM3-GC31-MM. A strong negative correlation ($r = -0.89$) is found between the amplitude of the changes in area and the mean position of the southern boundary. Although the focus is set on the southern boundary of the supergyre, the northern boundary is also found to shift poleward. The northern boundary shift appears to be greater than the southern boundary shift hence the area reduction. The supergyre normalized strength also increases in the future in all CMIP6 models apart from in UKESM1-0-LL and CAMS-CSM1-0 in which no change can be identified. In the majority of the CMIP6 models, no change in supergyre connectivity between the Indian and Pacific basins can be identified apart from BCC-CSM2-MR, CIESM, and HadGEM3-GC31-MM for which the supergyre, which was connected in the historical simulation is disconnected in the SSP5-8.5 scenario. It is unclear what the implications of the change in basin to basin connectivity are, especially given that the number of models for which there is a change is limited.

The changes in normalized strength, southern boundary, and area predicted by the CMIP6 models by the end of the century appear to be a continuation of some ongoing changes. Indeed, Qu et al. (2019) reported an observed intensification of the supergyre between 1993 and 2016 with the trends identifiable to a depth of at least 2,000 m.

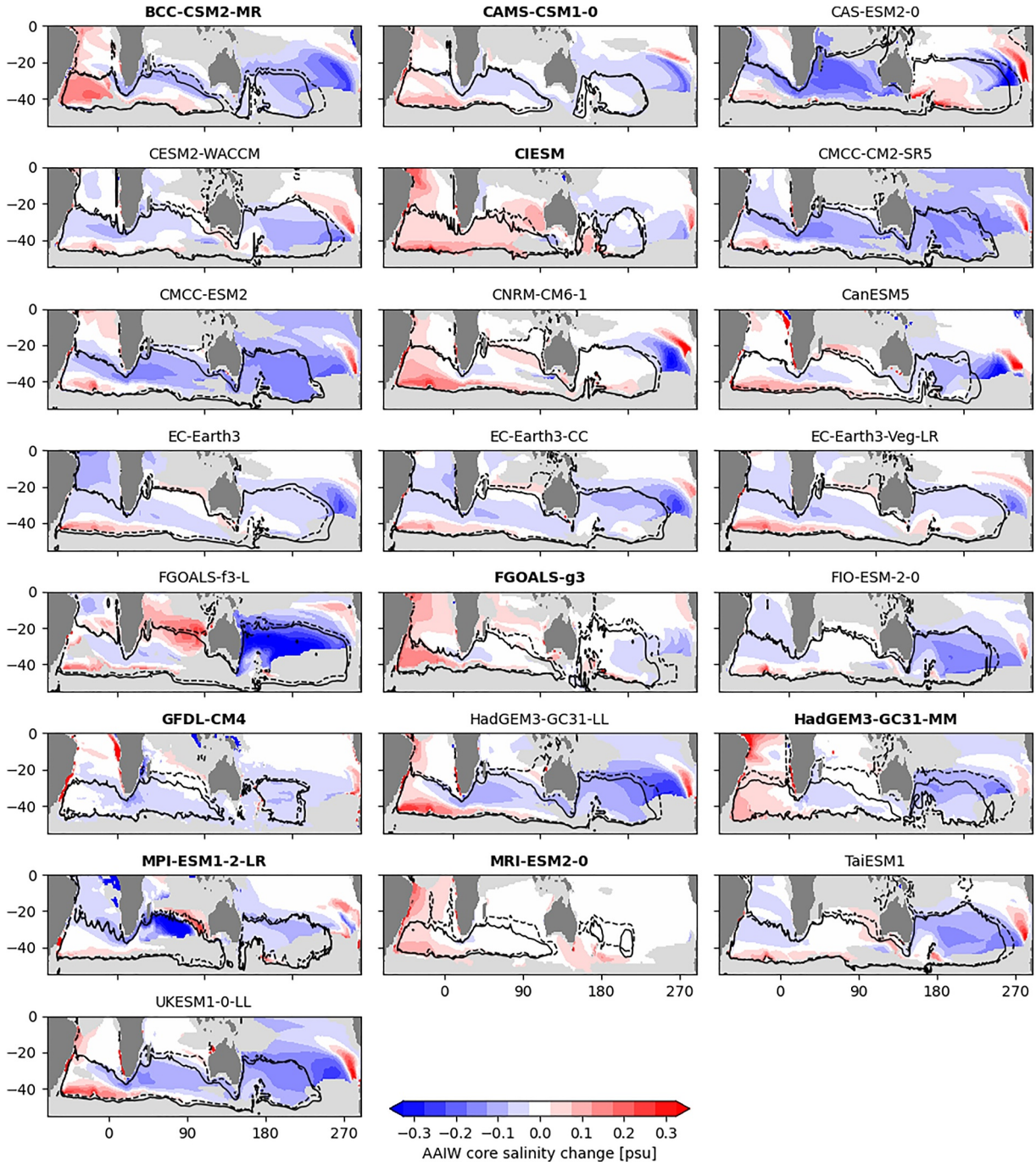

Figure 11. Difference in salinity at the Antarctic Intermediate Water core between the SSP5-8.5 and historical simulations. The black dashed (full) contour line corresponds to the supergyre contour in the intermediate layer in the historical (SSP5-8.5) simulation. Bold titles correspond to models with a disconnected supergyre in the SSPP5-8.5 simulation.

The future southward shift predicted by the CMIP6 models is also likely already happening, as a poleward shift of 2.5° was found in the SODA reanalysis product between 1958 and 2007 driven by a shift of the zero wind stress curl of about 3° (Duan et al., 2013). Furthermore, G. Wang et al. (2014) have highlighted the contribution of ozone depletion in the intensification and poleward shift of the supergyre in CMIP5 models under the RCP8.5 scenario. They showed that the poleward shift of the supergyre circulation was greatest during the ozone depletion period (1961–2005) compared to the ozone postrecovery period (2045–2100). This result could explain why the future

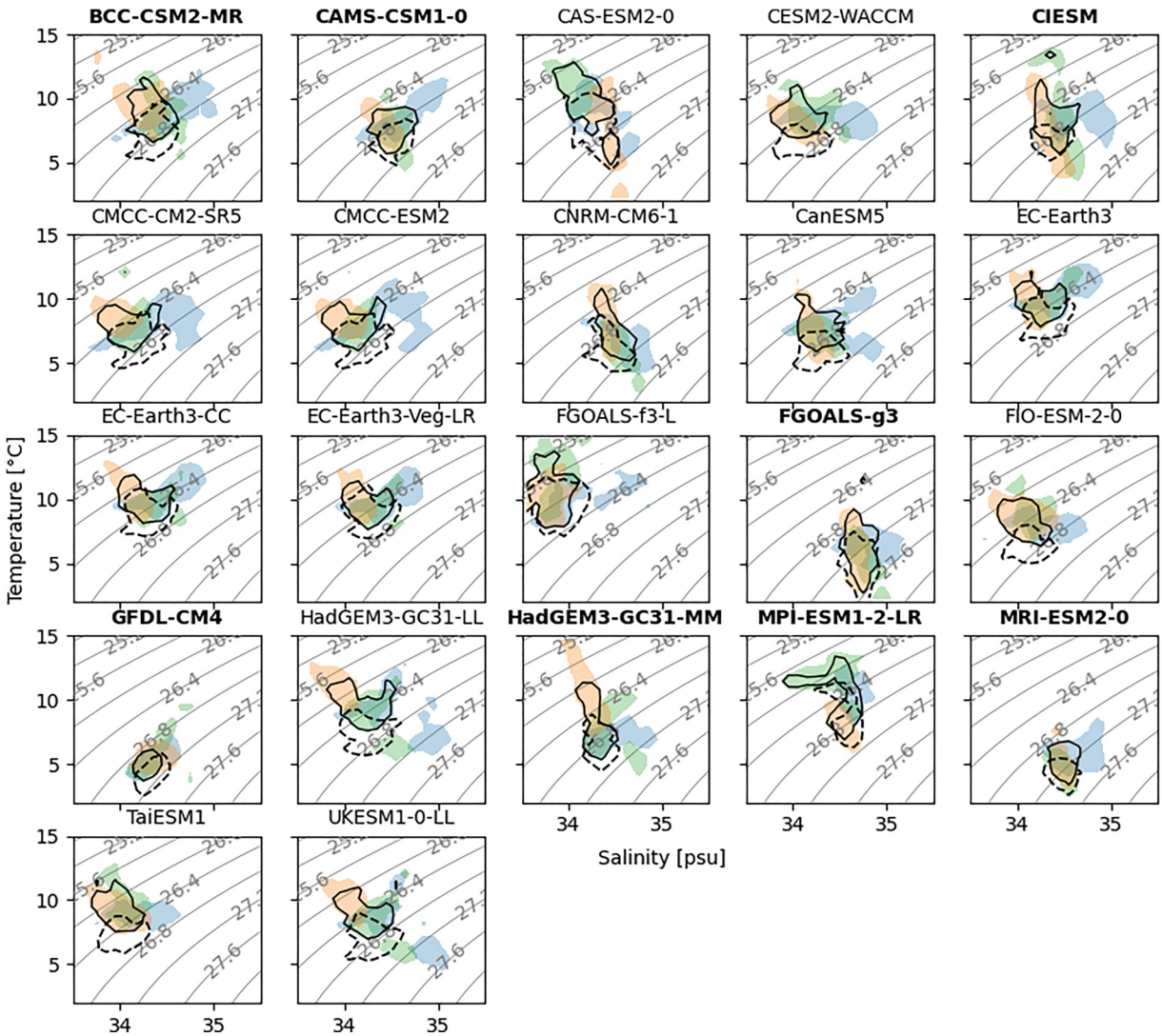

Figure 12. T/S diagram of the Antarctic Intermediate Water (AAIW) core temperature and salinity in the Pacific (orange), Indian (green), and Atlantic (blue) basins in the SSP5-8.5 simulations. The black line outlines the T/S values of the AAIW core within the supergyre in the SSP5-8.5 simulation. The dashed line represents the historical T/S values of the AAIW core within the supergyre as represented in Figure 8. Bold titles correspond to models with a disconnected supergyre in the SSP5-8.5 simulation.

poleward shift appears to slow down compared to the current shift diagnosed for instance in the SODA ocean reanalysis.

5.2. Future Changes in AAIW Core Properties

A poleward shift and intensification of the supergyre could influence the water mass exchanges between the basins. Using a high-resolution ocean-sea ice model, Biastoch et al. (2009) revealed that an increase in wind forcing can lead to an increase in AL, further resulting in a salinity increase in the South Atlantic. The relationship between the changes in supergyre properties (southern boundary shift and the change in strength) were compared to the changes in mean AAIW core temperature and salinity inside the supergyre but no statistically significant relationship could be found between the mean of the different quantities (not shown). The following subsection investigates whether patterns in temperature and salinity changes can be identified locally.

The AAIW core T/S values in the Southern Hemisphere for the SSP5-8.5 scenario are shown in Figure 12 and compared to the AAIW core T/S values within the supergyre in the historical simulation (black dashed line). Similarly to the historical period, in simulations forced by the SSP5-8.5 scenario, the supergyre corresponds to a

region of overlap between AAIW core T/S values in the Atlantic, Indian, and Pacific basins. The high degree of overlap suggests that the homogeneity in AAIW core T/S values found in the historical period is maintained in the future. In the majority of models, there is no major change in the spread of AAIW core T/S values found within the supergyre between the SSP5-8.5 and historical simulations with the exception of HadGEM3-GC31-MM, which presents a larger spread in *T* values and MPI-ESM1-2-LR, which presents a larger spread in S values within the supergyre in the future compared to the historical period.

All CMIP6 models show a warming of the supergyre, with a shift of the contour representing AAIW T/S core properties to warmer values (Figure 12), which is consistent with a lightening of the water masses circulating within the supergyre in all models. Although the changes in density appear to be dominated by temperature changes, changes in salinity of the AAIW core can also be identified (Figure 11). The changes vary both spatially and across models. Models are in agreement in the Pacific, where all models (apart from CAS-ESM2-0, CNRM-CM6-1, and MRI-ESM2-0) show a freshening of the AAIW core within the supergyre. In the Atlantic and Indian basins, patterns differ across both models and basins. A salinification of the AAIW core in the southern part of the supergyre in the Atlantic Basin can be identified in all CMIP6 models (apart from GFDL-CM4 in which there is no change in salinity). In the majority of models (16 out of 22), a smaller salinity change can be identified in the Indian Basin compared to the Atlantic, which suggests that the salinification originates in the Atlantic Basin and is advected eastward into the Indian Basin. In 8 out 22 CMIP6 models, the salinification at the AAIW core extends in the entirety of the supergyre in the Atlantic Basin. 13 out of 22 CMIP6 models show a salinification of the southern part and a freshening in the northern part of the supergyre in the Atlantic.

Figure 13 shows the change in temperature at the core of AAIW (as an anomaly to the spatial mean change of AAIW core temperature over the Southern Hemisphere which we refer to as relative change in temperature hereafter). Looking at the relative change in temperature is useful as it enables to identify which regions warm more than others. In some models, such as CESM2-WACCM, EC-Earth3, EC-Earth3-CC, EC-Earth3-Veg-LR, HadGEM3-GC31-LL, TaiESM1, and UKESM1-0-LL, the relative change in temperature is greater within the supergyre than outside of it. In CMCC-CM2-SR5 and CMCC-ESM2, the supergyre also coincides with a region of larger relative changes in temperature in the Pacific, although these models show no noticeable changes in the Atlantic. Models with a disconnected supergyre between the Pacific and Atlantic/Indian basins present differences in relative change in temperature between the Atlantic/Indian basins and the Pacific Basin with the exception of BCC-CSM2-MR and CAMS-CSM1-0. In CIESM, FGOALS-G3 and HadGEM3-GC31-MM, the Atlantic/Indian basins show a small negative relative change in temperature compared to the Pacific, where there is a positive relative change in temperature. In GFDL-CM4, MPI-ESM1-2-LR, and MRI-ESM2-0, the opposite pattern can be identified with positive relative change within the supergyre in the Atlantic/Indian basins compared to the negative or close to zero relative change in the Pacific. No clear patterns can be identified in CAS-ESM2-0 and FGOALS-f3-L with alternating positive/negative patterns in temperature relative change which could be due to the models' coarse vertical resolution (both models have only 30 vertical levels) that does not allow for a correct representation of the AAIW core and its future changes.

In summary, different responses of the AAIW core salinity to climate change are identified both spatially and across CMIP6 models. In contrast, we find that there is a consistent warming across the supergyre in all CMIP6 models. Interestingly, the patterns in T and S changes do not match spatially. It is unclear why the changes in salinity are not consistent across basins. Although a freshening of the properties at the outcrop of AAIW would be expected due to the increase in precipitation and ice melt in the future, no consistent freshening of the AAIW core is found. A similar result was found in the UKESM1-0-LL model where the outcrop position of AAIW was found to freshen at all longitudes; however, in the Atlantic, no consistent change in the salinity of the AAIW core was found (Meuriot et al., 2022).

6. Conclusions

The aim of the study was to investigate the influence of the supergyre on the properties and circulation of AAIW in 39 CMIP6 models and in the ECCO state estimate. The supergyre properties (position, area, strength, and connectivity) averaged between 1992 and 2011 were compared between the surface, intermediate, and deep layers defined around the AAIW core. The supergyre at the surface follows closely the zero wind stress curl and there is a good agreement in the position of the supergyre in ECCO and CMIP6 models. At intermediate depths, the majority of CMIP6 models (30 out of 39 models) present a supergyre connected through all basins whereas in

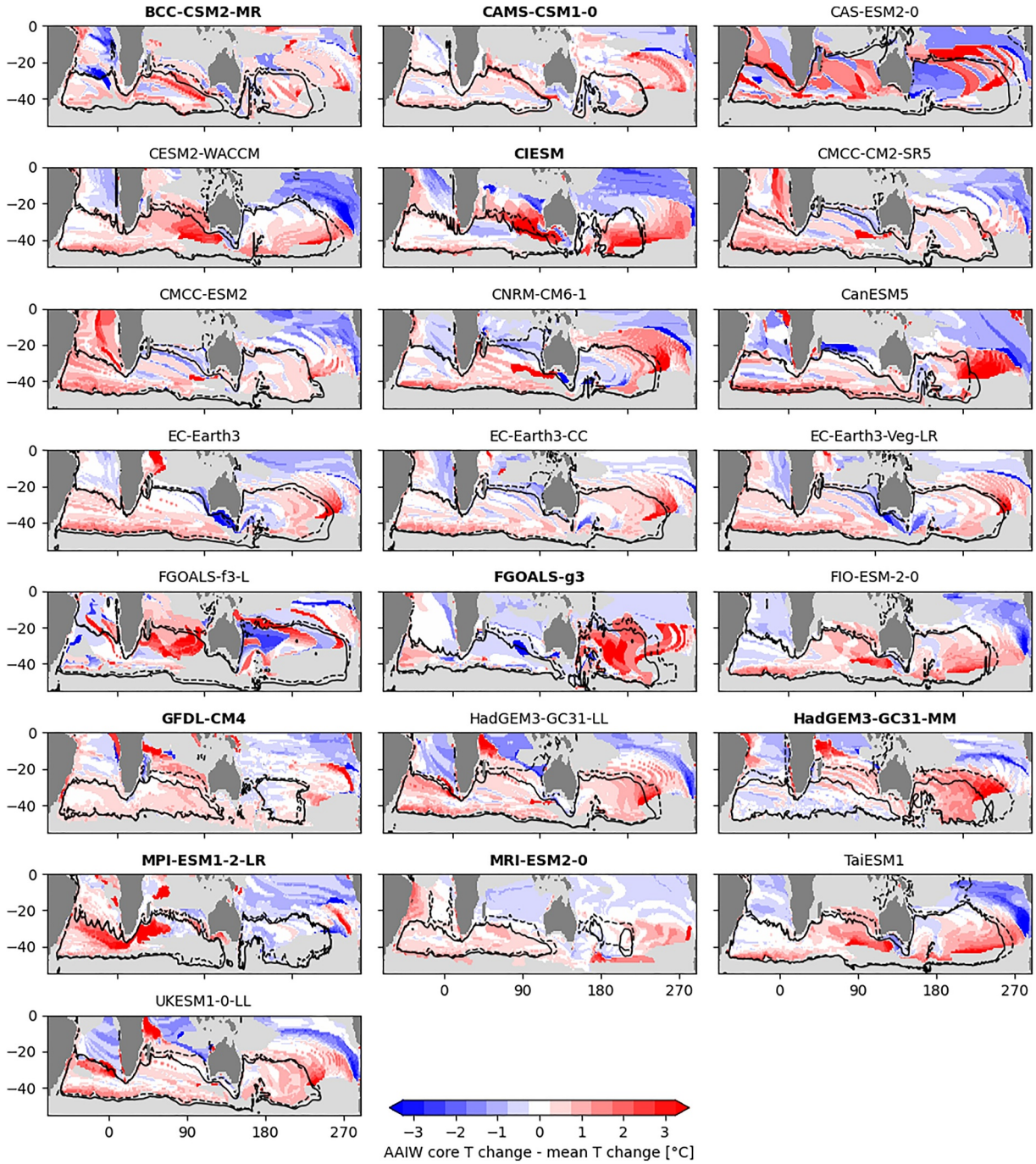

Figure 13. Change in temperature at the Antarctic Intermediate Water (AAIW) core between the SSP5-8.5 and historical simulations with the spatial mean change of the AAIW core temperature in the Southern Hemisphere subtracted. The black dashed (full) contour line corresponds to the intermediate supergyre contour in the historical (SSP5-8.5) simulation. Bold titles correspond to models with a disconnected supergyre in the SSP5-8.5 simulation.

ECCO and in 9 CMIP6 models, there is a disconnection between the Indian and Pacific basins. In the deep layer, the supergyre is very weak and disconnected between basins in most CMIP6 models and in ECCO.

The comparison of the supergyre at intermediate depths and AAIW properties showed that the supergyre position and AAIW core depth and salinity are interconnected. AAIW core is the deepest at the center of the supergyre where the streamfunction is the strongest. T/S at the AAIW core within the supergyre present similar values in the

Atlantic, Indian, and Pacific basins, suggesting that the supergyre plays a key role in homogenizing the AAIW properties.

In the future, although both changes in the supergyre properties and in AAIW properties are identified, the homogenization of AAIW properties within the supergyre is maintained when comparing the historical simulation (1992–2011 average) to the SSP5-8.5 scenario (2081–2100 average) in 22 CMIP6 models. The supergyre reduces in size and shifts poleward and intensifies. The core of AAIW warms in all CMIP6 models. The salinity patterns vary both spatially and across models. The AAIW core freshens in the Pacific in all CMIP6 models, however, in the Indian and Atlantic basins there is no consistent trend across models.

The lack of consistency across the CMIP6 models in the future change of the AAIW core salinity raises some questions on the potential implications of the changes. Graham et al. (2011) investigated the impact of a change in the AAIW core properties. The authors used experiments where a cooler/fresher and a warmer/saltier perturbation in AAIW was applied between 10°S and 20°S in the Atlantic while maintaining the density constant in HadCM3. In the case of the colder/fresher perturbation to the AAIW, Graham et al. (2011) found a decrease in the intensity of the meridional overturning circulation along with a decrease in sea surface temperature in the North Atlantic. The response to the warmer/saltier perturbation was not symmetric to the colder/fresher perturbation, highlighting the nonlinearity of the response to the perturbation, with also a decrease found in the intensity of the meridional overturning circulation, although of smaller magnitude, and no clear change of the sea surface temperature. The results by Graham et al. (2011) highlight that changes in AAIW properties can lead to changes in the meridional overturning circulation. In our study, however, the changes in temperature and salinity of the AAIW core are also associated with a lightening of the water mass due to the dominant contribution of the increase in temperature to the density change. It remains unclear how the changes identified will impact the meridional overturning circulation. Further work is needed to investigate the implications of the changes identified to the circulation in the Atlantic. In particular, it would be interesting to investigate the influence of the air-sea fluxes and their future changes on the properties of AAIW in order to gain some insights on the full life cycle of AAIW.

The study showed that the supergyre can be identified in CMIP6 models and that its structure varies with depth. As the majority of the CMIP6 models in the study have a resolution of 1 where eddies are parameterized, the next step would be to assess the role of an increase in resolution in the representation of the supergyre. Features such as the Agulhas Rings, which play a key role in the exchange of water masses between the Indian and Atlantic basins are not resolved in 1° models. An increase in resolution can also improve the large scale circulation with a better simulation of narrow currents and interaction with bathymetry. Further investigation is required to assess what the influence of model resolution is on the representation of the supergyre as well as on AAIW properties and circulation. In addition, the study here focused on a time averaged perspective. A high temporal and spatial resolution lagrangian tracking of the AAIW pathways could be beneficial to follow the temporal and local processes, which play a role in the interbasin circulation.

Future changes in the supergyre strength have also been linked with changes in the Atlantic Meridional Overturning Circulation (AMOC). Marcello et al. (2023) found that the weakening of the AMOC between 1920 and 2100 is associated with the spinning up of the Atlantic subtropical gyre in the Community Earth System Model 1 Large Ensemble simulation. They find that the AMOC weakens not because of a reduction in transport in TL or AL but rather because of more water being redirected southward in the subtropical gyre in the Atlantic. Further work is needed to assess the influence of the supergyre properties on the representation of the AMOC in CMIP6 models as well as to evaluate whether the relationship found in Marcello et al. (2023) between the intensification of the supergyre and the weakening of the AMOC is also happening in other CMIP6 models.

Data Availability Statement

The CMIP6 data was accessed through the Centre for Environmental Data Analysis (CEDA) archive and processed on JASMIN, the United Kingdom's data analysis facility for environmental science. The CMIP6 data can be downloaded on https://esgf-index1.ceda.ac.uk/projects/esgf-ceda/. The ECCO data used was the monthly product interpolated on a regular 720 × 1440 (latitude x longitude) grid which was accessed through the Physical Oceanography Distributed Active Archive Center (PODAAC): https://podaac.jpl.nasa.gov/ECCO.

Acknowledgments
This work was supported by the Grantham Institute and the UK NERC Science and Solution of a Changing Planet Doctoral Training Program at Imperial College London.

References

Biastoch, A., Böning, C. W., Schwarzkopf, F. U., & Lutjeharms, J. R. (2009). Increase in Agulhas leakage due to poleward shift of Southern Hemisphere westerlies. *Nature*, *462*(7272), 495–498. https://doi.org/10.1038/nature08519

Carmack, E. C. (2007). The alpha/beta ocean distinction: A perspective on freshwater fluxes, convection, nutrients and productivity in high-latitude seas. *Deep-Sea Research Part II Topical Studies in Oceanography*, *54*(23–26), 2578–2598. https://doi.org/10.1016/j.dsr2.2007.08.018

de Boyer Montégut, C., Madec, G., Fischer, A. S., Lazar, A., & Iudicone, D. (2004). Mixed layer depth over the global ocean: An examination of profile data and a profile-based climatology. *Journal of Geophysical Research*, *109*(12), 1–20. https://doi.org/10.1029/2004JC002378

Duan, Y., Hou, Y., Liu, H., & Liu, Y. (2013). The water mass variability and southward shift of the Southern Hemisphere mid-depth supergyre. *Acta Oceanologica Sinica*, *32*(11), 74–81. https://doi.org/10.1007/s13131-013-0380-7

Emery, W. J. (2001). Water types and water masses. In *Encyclopedia of ocean sciences* (pp. 3179–3187). https://doi.org/10.1006/rwos.2001.0108

Eyring, V., Bony, S., Meehl, G. A., Senior, C. A., Stevens, B., Stouffer, R. J., & Taylor, K. E. (2016). Overview of the Coupled Model Intercomparison Project Phase 6 (CMIP6) experimental design and organization. *Geoscientific Model Development*, *9*(5), 1937–1958. https://doi.org/10.5194/gmd-9-1937-2016

Feucher, C., Maze, G., & Mercier, H. (2019). Subtropical mode water and permanent pycnocline properties in the world ocean. *Journal of Geophysical Research: Oceans*, *124*(2), 1139–1154. https://doi.org/10.1029/2018jc014526

Forget, G., Campin, J. M., Heimbach, P., Hill, C. N., Ponte, R. M., & Wunsch, C. (2015). ECCO version 4: An integrated framework for non-linear inverse modeling and global ocean state estimation. *Geoscientific Model Development*, *8*(10), 3071–3104. https://doi.org/10.5194/gmd-8-3071-2015

Graham, J. A., Stevens, D. P., Heywood, K. J., & Wang, Z. (2011). North Atlantic climate responses to perturbations in Antarctic intermediate water. *Climate Dynamics*, *37*(1), 297–311. https://doi.org/10.1007/s00382-010-0981-1

Jiao, X., Zhang, J., Li, Q., & Li, C. (2022). Observational study on the variability of mixed layer depth in the Bering sea and the Chukchi sea in the summer of 2019. *Frontiers in Marine Science*, *9*(April), 1–13. https://doi.org/10.3389/fmars.2022.862857

Marcello, F., Tonelli, M., Ferrero, B., & Wainer, I. (2023). Projected Atlantic overturning slow-down is to be compensated by a strengthened South Atlantic subtropical gyre. *Communications Earth and Environment*, *4*(1), 92. https://doi.org/10.1038/s43247-023-00750-4

Meuriot, O., Lique, C., & Plancherel, Y. (2022). Properties, sensitivity, and stability of the Southern Hemisphere salinity minimum layer in the UKESM1 model. *Climate Dynamics*, *1*(1–2), 1–21. https://doi.org/10.1007/S00382-022-06304-2/METRICS

O'neill, B. C., Tebaldi, C., Van Vuuren, D. P., Eyring, V., Friedlingstein, P., Hurtt, G., et al. (2016). The scenario Model Intercomparison Project (ScenarioMIP) for CMIP6. *Geoscientific Model Development*, *9*, 3461–3482. https://doi.org/10.5194/gmd-9-3461-2016

Qu, T., Fukumori, I., & Fine, R. A. (2019). Spin-up of the Southern Hemisphere super gyre. *Journal of Geophysical Research: Oceans*, *124*(1), 154–170. https://doi.org/10.1029/2018JC014391

Ridgway, K. R., & Dunn, J. R. (2007). Observational evidence for a Southern Hemisphere oceanic supergyre. *Geophysical Research Letters*, *34*(13), 13612. https://doi.org/10.1029/2007GL030392

Roemmich, D., Gilson, J., Davis, R., Sutton, P., Wijffels, S., & Riser, S. (2007). Decadal spinup of the South Pacific subtropical gyre. *Journal of Physical Oceanography*, *37*(2), 162–173. https://doi.org/10.1175/JPO3004.1

Rosell-Fieschi, M., Rintoul, S. R., Gourrion, J., & Pelegrí, J. L. (2013). Tasman Leakage of intermediate waters as inferred from Argo floats. *Geophysical Research Letters*, *40*(20), 5456–5460. https://doi.org/10.1002/2013GL057797

Rousselet, L., Cessi, P., & Forget, G. (2020). Routes of the upper branch of the Atlantic meridional overturning circulation according to an ocean state estimate. *Geophysical Research Letters*, *47*(18), e2020GL089137. https://doi.org/10.1029/2020GL089137

Sallée, J. B., Shuckburgh, E., Bruneau, N., Meijers, A. J., Bracegirdle, T. J., Wang, Z., & Roy, T. (2013). Assessment of Southern Ocean water mass circulation and characteristics in CMIP5 models: Historical bias and forcing response. *Journal of Geophysical Research: Oceans*, *118*(4), 1830–1844. https://doi.org/10.1002/jgrc.20135

Schulzweida, U. (2022). *CDO user guide* (Vol. 10). Zenodo. https://doi.org/10.5281/zenodo.7112925

Speich, S., Blanke, B., & Cai, W. (2007). 12). Atlantic meridional overturning circulation and the Southern Hemisphere supergyre. *Geophysical Research Letters*, *34*(23). https://doi.org/10.1029/2007GL031583

Speich, S., Blanke, B., De Vries, P., Drijfhout, S., Döös, K., Ganachaud, A., & Marsh, R. (2002). Tasman leakage: A new route in the global ocean conveyor belt. *Geophysical Research Letters*, *29*(10), 55–61. https://doi.org/10.1029/2001gl014586

Wang, F., Xu, X., Zhang, F., & Ma, L. (2023). Structure of the Atlantic meridional overturning circulation in three generations of climate models. *Earth and Space Science*, *10*(7). https://doi.org/10.1029/2023EA002887

Wang, G., & Cai, W. (2013). Climate-change impact on the 20th-century relationship between the Southern Annular Mode and global mean temperature. *Scientific Reports*, *3*(1), 2039. https://doi.org/10.1038/srep02039

Wang, G., Cai, W., & Purich, A. (2014). Trends in Southern Hemisphere wind-driven circulation in CMIP5 models over the 21st century: Ozone recovery versus greenhouse forcing. *Journal of Geophysical Research: Oceans*, *119*(5), 2974–2986. https://doi.org/10.1002/2013JC009589

Zhang, H., Menemenlis, D., & Fenty, I. (2018). ECCO LLC270 ocean-ice state estimate.